Article

SOURCE DATA | TRANSPARENT PROCESS

THE EMBO JOURNAL

Rac1-Rab11-FIP3 regulatory hub coordinates vesicle traffic with actin remodeling and T-cell activation

Jérôme Bouchet[1,2,3,*,†], Iratxe del Río-Iñiguez[1,2,3], Rémi Lasserre[1,2,‡], Sonia Agüera-Gonzalez[1,2,§], Céline Cuche[1,2,3], Anne Danckaert[4], Mary W McCaffrey[5], Vincenzo Di Bartolo[1,2,3] & Andrés Alcover[1,2,3,**]

Abstract

The immunological synapse generation and function is the result of a T-cell polarization process that depends on the orchestrated action of the actin and microtubule cytoskeleton and of intracellular vesicle traffic. However, how these events are coordinated is ill defined. Since Rab and Rho families of GTPases control intracellular vesicle traffic and cytoskeleton reorganization, respectively, we investigated their possible interplay. We show here that a significant fraction of Rac1 is associated with Rab11-positive recycling endosomes. Moreover, the Rab11 effector FIP3 controls Rac1 intracellular localization and Rac1 targeting to the immunological synapse. FIP3 regulates, in a Rac1-dependent manner, key morphological events, like T-cell spreading and synapse symmetry. Finally, Rab11-/FIP3-mediated regulation is necessary for T-cell activation leading to cytokine production. Therefore, Rac1 endosomal traffic is key to regulate T-cell activation.

Keywords actin cytoskeleton; immunological synapse; intracellular traffic; Rab11-FIP3; Rac1; recycling endosomes

Subject Categories Cell Adhesion, Polarity & Cytoskeleton; Immunology; Membrane & Intracellular Transport

DOI 10.15252/embj.201593274 | Received 14 October 2015 | Revised 2 March 2016 | Accepted 5 April 2016 | Published online 6 May 2016

The EMBO Journal (2016) 35: 1160–1174

Introduction

T cells recognize antigens as molecular fragments associated with major histocompatibility complex molecules expressed on the surface of antigen-presenting cells (APC). This triggers a massive T-cell polarization process toward the APC, leading to the generation of an organized cell–cell junction named the immunological synapse (Agüera-Gonzalez *et al*, 2015). T-cell receptor (TCR) signal transduction induces the reorganization of both the actin and microtubule cytoskeleton. Thus, actin actively polymerizes at the periphery of the synapse in a finely regulated manner (Bunnell *et al*, 2001; Roumier *et al*, 2001; reviewed in Burkhardt *et al*, 2008). Moreover, T-cell microtubules reorient and radially organize, bringing the centrosome close to the synapse, through a mechanism depending on the cortical actin-associated protein ezrin and the polarity regulator Dlg1 (Lasserre *et al*, 2010). Actin and microtubule rearrangements are necessary for signaling complex dynamics at the immunological synapse and for T-cell activation (Valitutti *et al*, 1995; Campi *et al*, 2005; Nguyen *et al*, 2008; Lasserre *et al*, 2010; Hashimoto-Tane *et al*, 2011). TCR signaling controls actin cytoskeleton dynamics via a network of regulatory proteins, including the Rho-family GTPases Rac1 and Cdc42, activated by their guanine exchange factor Vav1 (Hornstein *et al*, 2004; Burkhardt *et al*, 2008).

Polarized vesicle traffic also contributes to the generation and function of the immunological synapse. The Golgi apparatus reorients to the synapse and delivers helper cytokines to the APC (Kupfer *et al*, 1991). Moreover, several types of endosomal vesicles deliver the TCR, the tyrosine kinase Lck and the signaling adapter LAT to the immunological synapse in a differentially regulated manner. Indeed, Lck, TCRζ, and LAT are associated with endosomal vesicular compartments whose traffic is controlled by different regulators, including Rab GTPases, intraflagellar transport proteins, and SNAREs. Perturbation of these regulatory proteins impairs immunological synapse formation and function (Das *et al*, 2004; Anton *et al*, 2008; Patino-Lopez *et al*, 2008; Finetti *et al*, 2009, 2015; Martin-Cofreces *et al*, 2012; Larghi *et al*, 2013; Soares *et al*, 2013a).

1 Lymphocyte Cell Biology Unit, Department of Immunology, Institut Pasteur, Paris, France
2 CNRS URA 1961, Paris, France
3 INSERM U1221, Paris, France
4 Institut Pasteur Citech-Imagopole, Paris, France
5 Molecular Cell Biology Laboratory, Biosciences Institute, School of Biochemistry and Cell Biology, University College Cork, Cork, Ireland
*Corresponding author. E-mail: jerome.bouchet@inserm.fr
**Corresponding author. E-mail: andres.alcover@pasteur.fr
† Present address: Institut Cochin INSERM, U1016, CNRS, UMR8104, Sorbonne Paris Cité, Université Paris Descartes, Paris, France
‡ Present address: Centre d'Immunologie de Marseille Luminy, Université Aix-Marseille, CNRS UMR7280, INSERM U1104, Marseille, France
§ Present address: Institut Curie, Membrane and Cytoskeleton Dynamics Group, CNRS UMR144, Paris, France

Initial TCR signaling triggers both cytoskeleton reorganization and polarized endosomal vesicle traffic that cooperate to build immunological synapses able to regulate sustained TCR activation (Soares *et al*, 2013b). However, how TCR signaling, cytoskeleton rearrangements, and endosomal traffic are coordinated is poorly known. Here, we show that Rab11 recycling endosomes play a pivotal role in this orchestration. Rab11 regulates, through the interaction with its effector Rab11-FIP3 (Horgan & McCaffrey, 2009), the subcellular localization of the GTPase Rac1 in resting T cells, and its targeting to the immunological synapse. Rac1 localization, in turn, is crucial to control T-cell spreading, immunological synapse symmetry, and ultimately T-cell activation leading to cytokine production.

Results

Rab11-FIP3 controls Rac1 subcellular localization in recycling endosomes and Rac1 clustering at the immunological synapse

As a first approach to investigate the relationship between polarized endosomal traffic and actin cytoskeleton reorganization at the immunological synapse, we investigated the subcellular localization of Rab11 and Rac1, two GTPases that are master regulators of endosomal recycling (Welz *et al*, 2014) and cortical actin dynamics (Steffen *et al*, 2014), respectively. Interestingly, we observed a significant amount of Rac1 colocalized with Rab11 in the pericentrosomal compartment, while the rest of Rac1 was at the cell cortex and dispersed in the cytosol (Fig 1A, top, and B).

To investigate whether Rab11 regulates Rac1 endosomal localization, we analyzed the involvement of Rab11-family interacting proteins (FIPs). These are five effectors, key for Rab11 regulation of endosomal traffic (Horgan & McCaffrey, 2009). Among them, FIP3 interactions with traffic and cytoskeleton regulators, including dynein (Horgan *et al*, 2010) and Arf6 (Fielding *et al*, 2005), prompted us to study this effector. Consistently with previous observations (Horgan *et al*, 2007), FIP3 silencing by two different siRNA strongly perturbed the structural integrity of the Rab11-endosomal-recycling compartment. Importantly, FIP3 silencing altered Rac1 pericentrosomal localization, fragmenting it into smaller vesicles located all over the cytoplasm and strongly reducing Rab11-Rac1 colocalization (Fig 1A, bottom, and B). FIP3 silencing did not change the total levels of Rac1 (Fig 2A and B), ruling out that Rac1 disappearance from the pericentrosomal compartment was followed by Rac1 degradation.

Conversely, overexpression of FIP3 wild type (WT) strongly concentrated Rac1 in the endosomal compartment, where both molecules strongly colocalized (Fig 1E, middle, and F). In contrast, the overexpression of a FIP3-I^{378}E mutant, displaying a single amino acid substitution in the FIP3 Rab11-binding domain (Fig 1D) that impairs its interaction with Rab11 (Horgan *et al*, 2010), delocalized Rac1 from the endosomal compartment to the cytosol and the cell cortex (Fig 1E, bottom). Consistently, Rac1 significantly colocalized in endosomes with Rab11WT and with the Rab11 active mutant (GTP-bound, Q^{70}L). In contrast, the dominant negative mutant (GDP-bound, S^{25}N) altered endosomal Rac1 localization and poorly colocalized with it (Fig 1G and H).

These data indicate that FIP3 may regulate Rac1 subcellular localization. This prompted us to investigate whether FIP3 and Rac1 interact. To this end, we overexpressed GFP, GFP-FIP3WT, or the GFP-FIP3I^{738}E mutant in HEK293T cells and carried out anti-GFP immunoprecipitation and Rac1 Western blot analyses of the different cell lysates. Rac1 was weakly but reproducibly found to be associated with GFP-FIP3 and to a lesser extent with GFP-FIP3I^{738}E mutant, but failed to associate with GFP alone (Fig 2C).

Subsequently, we investigated the effect of FIP3 on Rac1 targeting to the immunological synapse. In control cells, Rac1 clustered across the immunological synapse, which significantly diminished in cells overexpressing FIP3WT or FIP3I^{738}E (Fig 3A and C). In contrast, neither the overexpression of Rab11WT, Rab11Q^{70}L, or Rab11S^{25}N (Fig 3B and C), nor FIP3 silencing with siRNA (Fig 3D and E), significantly diminished the amount of Rac1 targeted to the synapse. TCR-CD3 clustering, as assessed by anti-CD3ε (Fig 3D), or anti-phospho-TCRζ (not shown), was also readily observed at the synapse of FIP3-silenced cells, partially overlapping with the Rac1 cluster.

Altogether, these data indicate that Rac1 subcellular localization, intracellular traffic, and targeting to the immunological synapse occur via the Rab11-endosomal-recycling compartment and are regulated by Rab11-FIP3.

Rab11-FIP3 regulates immunological synapse symmetry and size

During immunological synapse formation, T cells spread, forming a symmetric lamellipodium-like structure, which relies on

Figure 1. Rac1 is associated with Rab11-positive recycling endosomes.

A–C Jurkat T cells were transfected with control, FIP3.1, or FIP3.2 siRNA oligonucleotides. (A) Intracellular distribution of endogenous Rab11 and Rac1 was assessed by immunofluorescence. (B) Pearson's correlation coefficients between Rab11 and Rac1 staining are shown, each dot represents one single cell. (C) FIP3 expression was analyzed by Western blot. Quantification of bands was performed with ImageJ and normalized to a non-specific band of 35 kDa used as a loading control.

D Schematic representation of FIP3 structural features: proline-rich region, EF-hand domain, coiled-coil domain (CC), Arf-binding domain (ABD), and Rab-binding domain (RBD).

E, F Jurkat cells were transfected with expression vectors encoding GFP, GFP-FIP3-WT, or GFP-FIP3-I^{738}E. (E) Endogenous Rac1 was detected by immunofluorescence. (F) Pearson's correlation coefficients between FIP3WT and Rac1 stainings are shown, each dot represents one single cell.

G, H Jurkat cells were transfected with expression vectors encoding GFP, Rab11WT-GFP, or Rab11Q^{70}L-GFP (constitutively active) or Rab11S^{25}N-GFP (dominant negative) mutants. (G) Endogenous Rac1 was detected by immunofluorescence. (H) Pearson's correlation coefficients between Rab11 and Rac1 staining are shown, each dot represents one single cell.

Data information: (A, E, G) Three-dimensional (3D) confocal images were post-treated by deconvolution. A 0.4-μm-thick medial stack is shown. The pericentrosomal vesicular compartment is zoomed at the bottom right-hand corner. Scale bars, 5 μm. (B, F, H) Population analysis of the co-localization volume between Rab11 and Rac1 within the pericentriolar vesicular compartment. Horizontal bars represent the mean ± SEM, Mann–Whitney *U*-test was used. Images are representative of three experiments.
Source data are available online for this figure.

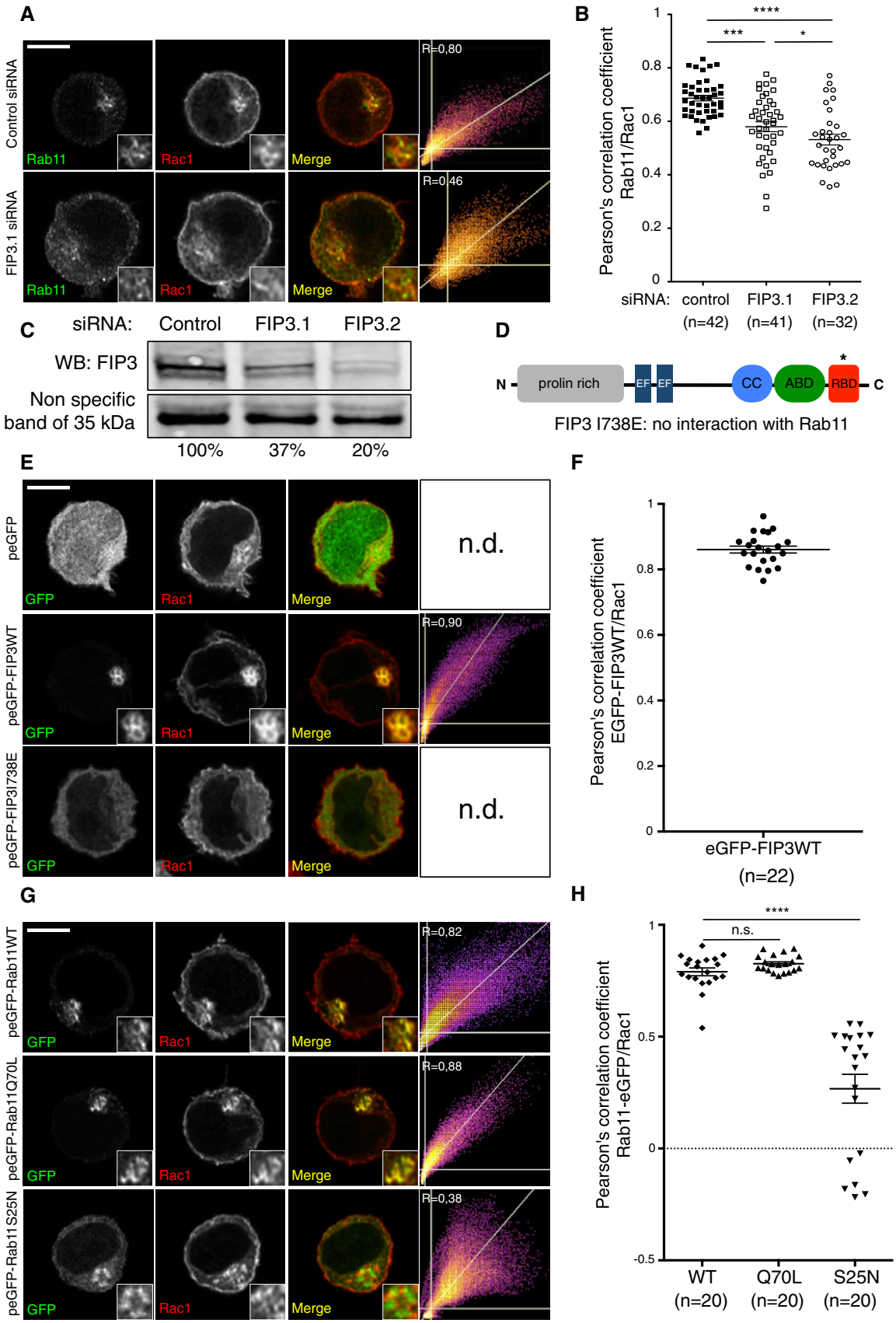

Figure 1.

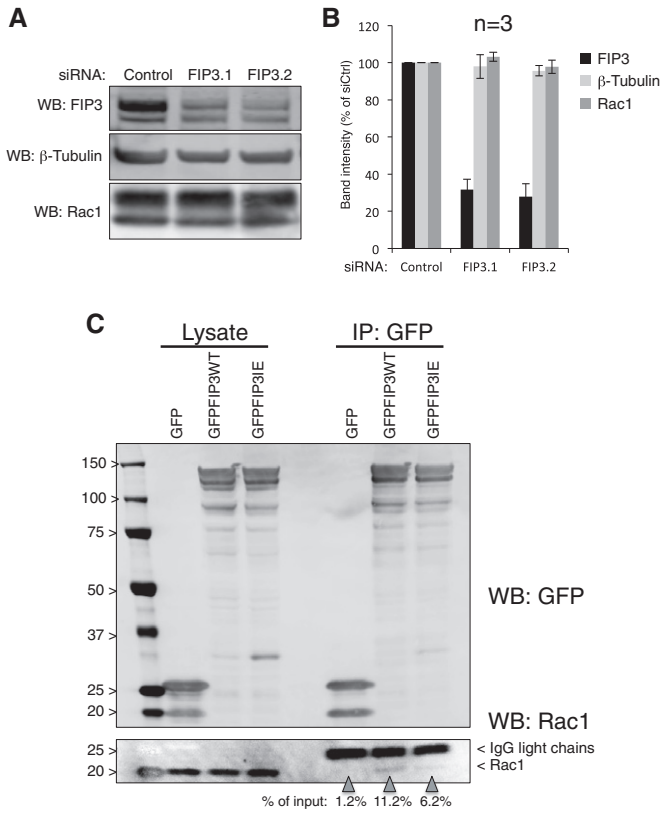

Figure 2. Rac1 interaction with FIP3 and effect of FIP3 silencing on Rac1 expression.

A, B Effect of FIP3 silencing on Rac1 expression. Jurkat cells were transfected with control, FIP3.1, or FIP3.2 siRNA. Three days later, cells were lysed and the expression of FIP3, Rac1, and β-tubulin were analyzed by Western blot. The intensity of bands corresponding to FIP3 and to Rac1 was quantified by ImageJ and normalized to the β-tubulin band used as a loading control. The mean ± SD of the percentage of band intensity in silenced cells with respect to controls of three independent experiments is shown.

C Rac1 interaction with FIP3. HEK293T cells were transfected with GFP, GFP-FIP3 WT, or GFP-FIP3I^{738}E expression vectors. Twenty-four hours later, cells were lysed and immunoprecipitated with anti-GFP Ab. Immunoprecipitates were analyzed by electrophoresis and Western blot using anti-GFP Ab (top panel) or anti-Rac1 Ab (bottom panel). Total cell lysates were analyzed (100,000 cells). The position of Rac1 (20 kDa) and Ig light chain (25 kDa) polypeptides is depicted on the right side. Arrowheads at the bottom point the bands corresponding to Rac. Quantification of bands was performed with ImageJ as the percentage of intensity with respect to the total lysate bands on the left, shown below. A representative experiment out of three carried out is shown.

Source data are available online for this figure.

TCR-induced Rac1- and WASP-dependent actin dynamics (Bunnell *et al*, 2001; Sims *et al*, 2007; Le Floc'h *et al*, 2013 and references therein). We hypothesized that Rab11 endosomes could condition Rac1 subcellular localization and, as a consequence, actin dynamics driving T-cell spreading and immunological synapse formation. Indeed, while control cells formed symmetric immunological synapses with superantigen (sAg)-pulsed APCs, FIP3-silenced T cells formed strongly asymmetric synapses (Fig 4A). To assess this phenomenon, we measured the angle formed by an axis binding the synapse edges and another one connecting the mass centers of the T cell and the APC nuclei (Materials and Methods and Fig 4B). While control synapses formed angles very close to 90°, FIP3-silenced cells displayed significantly narrower angles (Fig 4C).

We next analyzed the capacity of T cells to spread in response to TCR-CD3 stimulation, analyzing the contact sites formed by T cells on anti-CD3-coated coverslips (Lasserre *et al*, 2010). The absence of APC surface constraints in these "pseudosynapses" allows more accurate measurements of cell spreading. Interestingly, FIP3-silenced T cells spread faster and to a larger extent than control cells (Fig 4D–F).

These data show that Rab11-FIP3-regulated endosomal recycling regulates T-cell spreading and immunological synapse symmetry, suggesting that Rac1 endosomal traffic could mediate these effects.

Rab11-FIP3 regulates T-cell spreading independently of TCR engagement

Endosomal traffic of TCR, Lck, and LAT regulates immunological synapse formation and function (Das *et al*, 2004; Finetti *et al*, 2009; Larghi *et al*, 2013; Soares *et al*, 2013a). Moreover, T-cell spreading and actin dynamics are regulated by TCR signaling in an Lck- and LAT-dependent manner (Bunnell *et al*, 2001). To discriminate whether changes in T-cell spreading and synapse symmetry induced by FIP3 silencing were the consequence of TCR proximal signaling modifications, or the direct influence of Rac1-mediated regulation of these phenomena, we analyzed T cells dropped on poly-lysine-coated coverslips. Control T cells adhered to the poly-lysine surface, but only moderately spread, or formed F-actin-rich lamellipodia (Fig 5A top, B and C). This is consistent with a non-specific adhesion phenomenon independent of TCR or integrin signaling. Strikingly, FIP3-silenced cells spread more efficiently on poly-lysine, displaying larger membrane extensions in both Jurkat (Fig 5A–C) and primary T cells (Fig 5D and E), in which enhanced F-actin could be observed (Fig 5A bottom). Worth noting, cell spreading on poly-lysine was inversely proportional to the amount of FIP3 present in the cells, as assessed by transfecting different doses of FIP3 siRNA (Appendix Fig S1).

T-cell spreading depends on cortical cytoskeleton dynamics that in turn condition cell rigidity. To assess the influence of Rab11-FIP3 silencing in T-cell rigidity, we analyzed the resistance of primary T cells to be distorted by centrifugation (Faure *et al*, 2004) (see Materials and Methods). Consistent with the spreading data, FIP3-silenced cells were significantly more deformable than control cells (Fig 5F), suggesting that cellular rigidity was diminished in FIP3-silenced cells. These findings are in line with those by Faure *et al*, showing that cellular rigidity was reduced by Rac1 activity (Faure *et al*, 2004).

These results suggest that Rab11-FIP3 regulates T-cell spreading and cortical rigidity by controlling Rac1 localization, and actin remodeling independently of TCR signaling.

Rab11-FIP3 regulates T-cell spreading and immunological synapse symmetry via a Rac1-dependent mechanism

To further investigate whether FIP3-dependent modulation of T-cell spreading was the result of Rac1 localization, we co-transfected control or siFIP3 oligonucleotides, together with expression vectors encoding Rac1WT, constitutively active Rac1G^{12}V, or dominant negative Rac1T^{17}N mutants. The capacity of cells to spread on poly-lysine-coated coverslips was then assessed as in Fig 5. Rac1WT

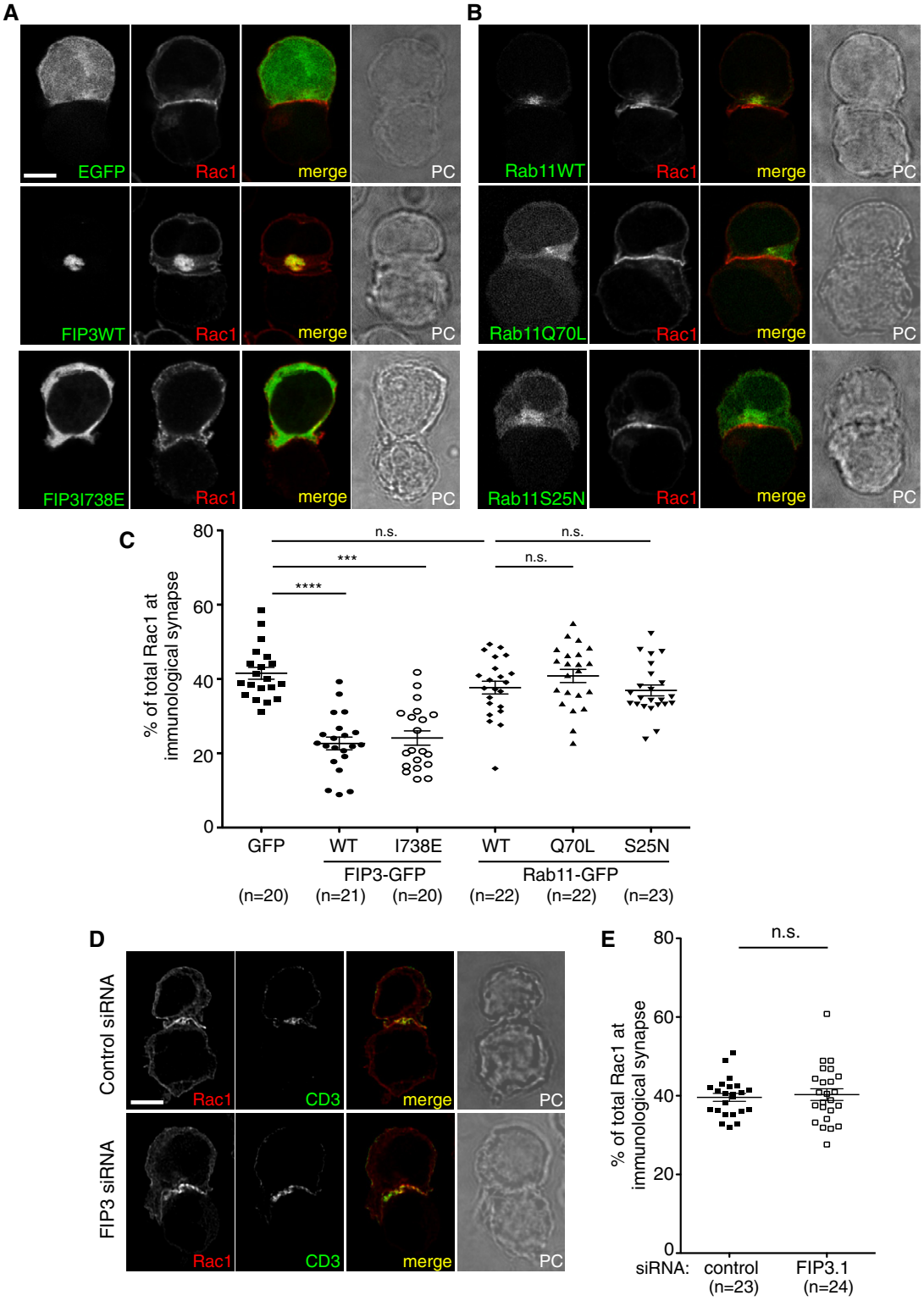

Figure 3. Rab11-FIP3 controls Rac1 clustering at the immunological synapse.

A–E Jurkat T cells were transfected with expression vectors encoding: (A, C) GFP, GFP-FIP3WT, or GFP-FIP3I^{738}E; (B, C) Rab11WT-GFP, Rab11Q^{70}L-GFP (constitutively active), or Rab11S^{25}N-GFP (dominant negative); or transfected with (D, E) control or FIP3.1 siRNA. Cells were allowed to form immunological synapses with SEE-pulsed Raji cells for 30 min. Intracellular distribution of endogenous Rac1 and surface distribution of CD3 were detected by immunofluorescence. 3D confocal images were post-treated by deconvolution. A 0.4-μm-thick medial stack is shown. (C, E) Population analyses of the amount of Rac1 at the immunological synapse relative to the total cellular Rac1. Each dot corresponds to one cell. Horizontal bars represent the mean ± SEM. Mann–Whitney *U*-test. ***$P < 0.001$, ****$P < 0.0001$. Images are representative of three experiments. Scale bars, 5 μm.

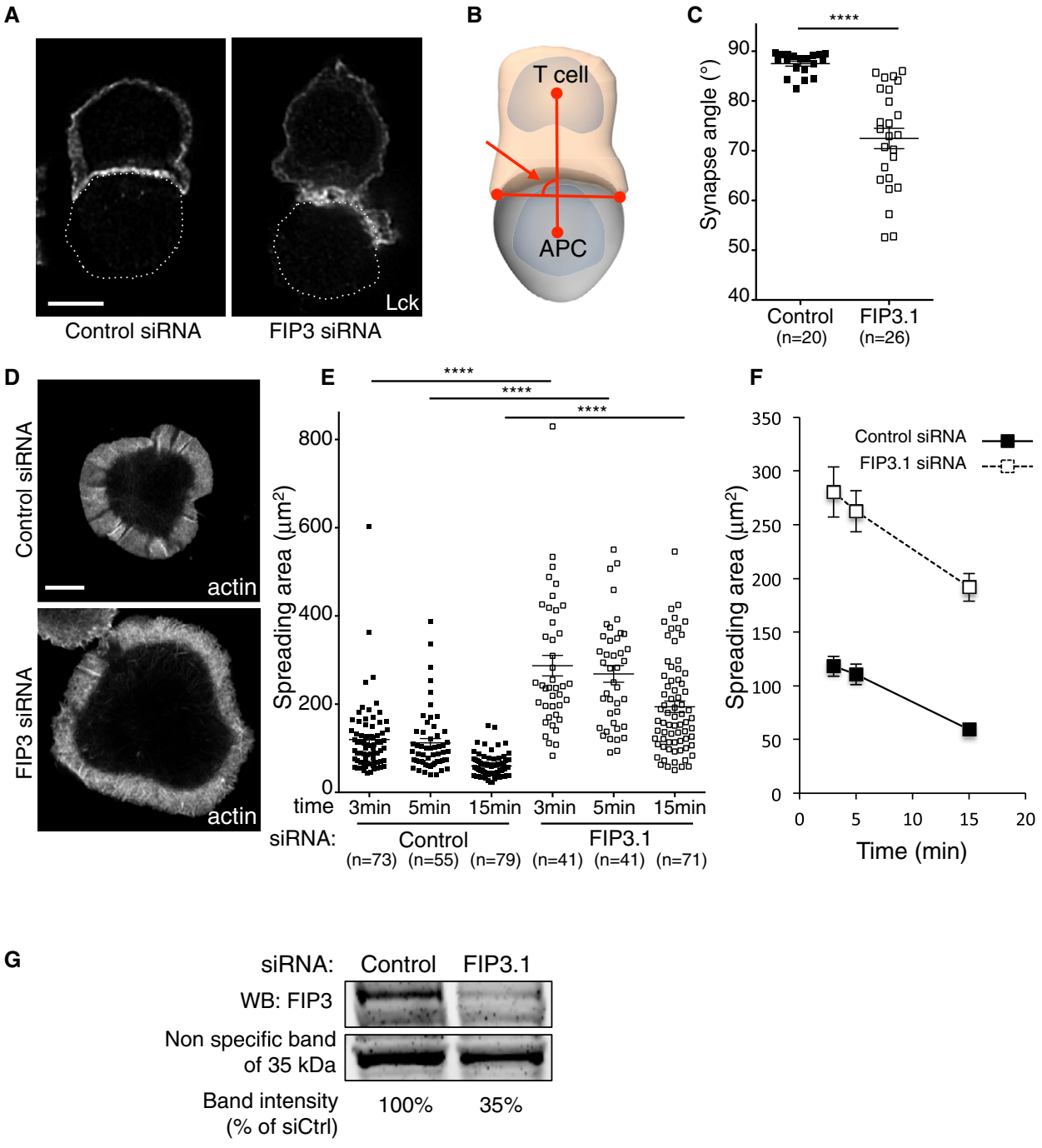

Figure 4. Rab11-FIP3 regulates immunological synapse symmetry and size.
Jurkat T cells were transfected with either control or FIP3.1 siRNA.

A Cells were allowed to form immunological synapses with SEE-pulsed Raji cells for 30 min, and endogenous Lck was detected by immunofluorescence. 3D confocal images were post-treated by deconvolution. A 0.4-µm-thick medial stack is shown. Scale bar, 5 µm.

B, C The minimal angle formed by the axis connecting the synapse edges and the axis connecting the mass centers of the T cell and the APC nuclei was measured, as schematized in (B). Horizontal bars represent the mean ± SEM. Mann-Whitney *U*-test. ****$P < 0.0001$. Images are representative of three experiments.

D Transfected Jurkat T cells were allowed to spread on anti-CD3-coated coverslips for the indicated time, and F-actin was detected with FITC-phalloidin. A single optical section at the level of the contact surface is shown. Scale bar, 10 µm.

E, F Population analyses of the spreading area of cells at the level of the contact surface. Each dot corresponds to one cell. Horizontal bars represent the mean ± SEM. Mann–Whitney *U*-test. ****$P < 0.0001$. Images are representative of three experiments.

G FIP3 expression was analyzed by Western blot. Quantification of bands was performed with ImageJ and normalized to a non-specific band of 35 kDa used as a loading control.

Source data are available online for this figure.

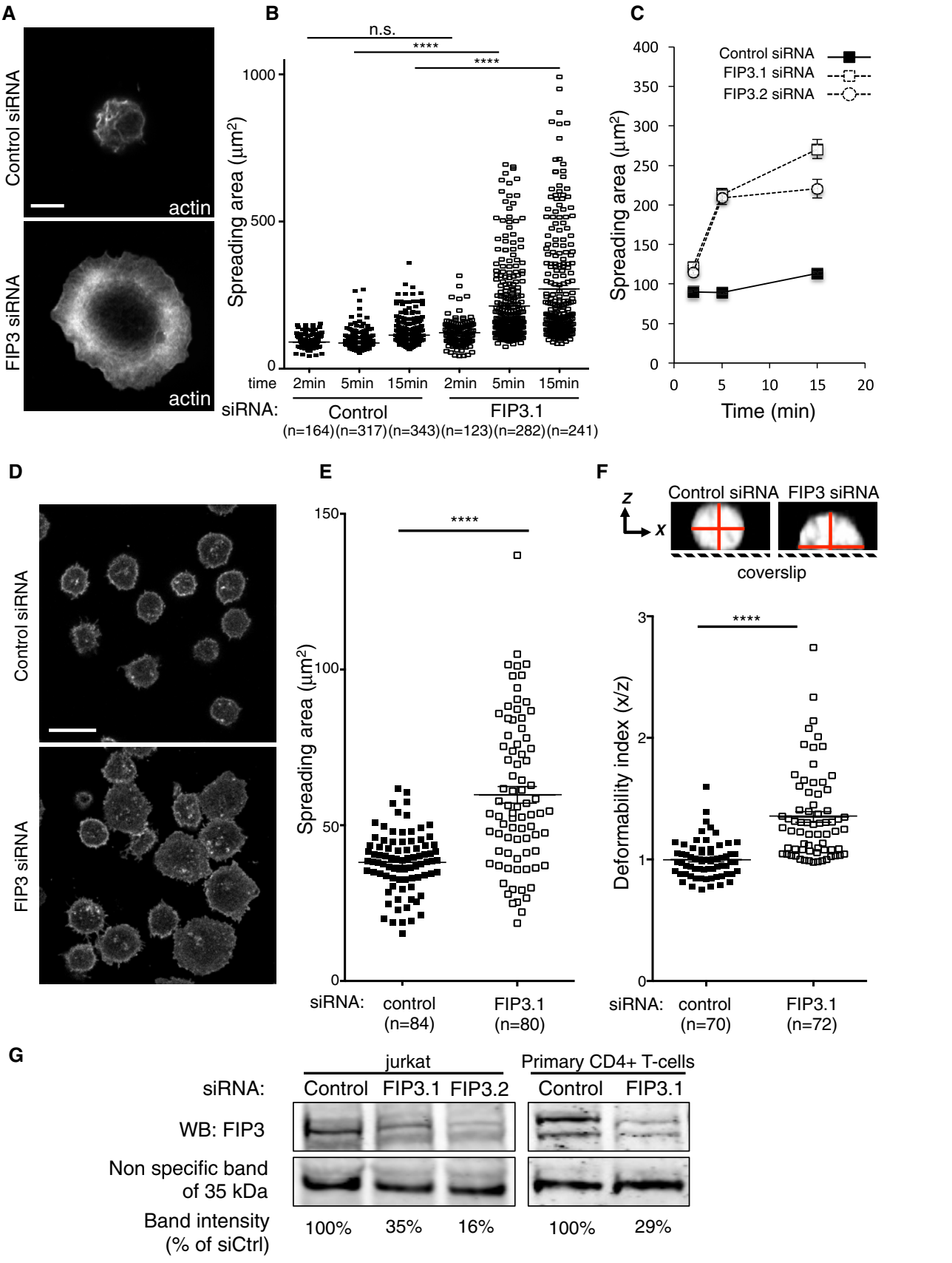

Figure 5.

Figure 5. Rab11-FIP3 regulates T-cell spreading and cortical rigidity independently of TCR engagement.

A–C Jurkat T cells transfected with siRNA control, FIP3.1, or FIP3.2 were allowed to spread on poly-lysine-coated coverslips for the indicated times. Intracellular actin was detected with FITC-coupled phalloidin. (A) A single optical section at the level of the contact surface is shown. Scale bar, 5 μm. (B) Population analyses of the spreading area of cells at the level of the contact surface. Each dot represents one cell. Horizontal bars represent the mean ± SEM. Mann–Whitney *U*-test. ****$P < 0.0001$. (C) Time course representation of (B), showing mean ± SEM. Images are representative of three experiments.

D–F Primary human CD4 T cells were transfected with control or FIP3.1 siRNA. (D, E) Cells were allowed to spread on poly-lysine-coated coverslips for 5 min. Intracellular Lck was detected by immunofluorescence. (D) A single optical section at the level of the contact surface is shown. Scale bar, 10 μm. (E) Population analyses of the spreading area of cells at the level of the contact surface. (F) Cells were stained with CMFDA dye, suspended in a paraformaldehyde solution, and submitted to centrifugation at 3,724 × *g* onto poly-lysine-coated coverslips. Confocal optical sections separated by 0.2 μm were acquired. *X-Z* images were built with ImageJ. The maximal sections in "x" (width) and "z" (thickness) were determined for each cell (upper panel). Plots represent the deformability index (x/z). Each dot corresponds to one cell. Horizontal bars represent the mean ± SEM. Mann–Whitney *U*-test. ****$P < 0.0001$. Images are representative of three experiments.

G FIP3 expression was analyzed by Western blot. Quantification of bands was performed with ImageJ and normalized to a non-specific band of 35 kDa used as a loading control.

Source data are available online for this figure.

overexpression increased the spreading ability of control cells to a lesser extent than FIP3 silencing and did not increase FIP silencing effect (Fig 6A, E and H). Overexpression of the constitutively active Rac1G^{12}V mutant efficiently increased spreading of control as well as of FIP3-silenced cells (Fig 6B, F and H). Conversely, the dominant negative Rac1T^{17}N mutant significantly inhibited the spreading ability of FIP3-silenced cells, also reducing the moderate spreading capacity of control cells (Fig 6C, G and H).

To further proof the Rac1 dependence of FIP3 silencing effects on T-cell spreading and immunological synapse symmetry, we used a specific Rac1 inhibitor (NSC23766), which competes the ability of Rac1 to interact with its guanine exchange factors (GEFs), thus preventing Rac1 activation, without affecting Rho or Cdc42 (Gao *et al*, 2004). Indeed, this inhibitor reverted both FIP3 silencing effects on cell spreading and synapse symmetry (Fig 7A and B).

Altogether, these data indicate that Rab11-FIP3-regulated endosomal recycling controls Rac1 subcellular localization and its ability to control actin cytoskeleton dynamics, with consequences on T-cell spreading and immunological synapse symmetry. Therefore, lamellipodia formation at the immunological synapse appears to be tuned by Rac1 localization via recycling endosomes.

FIP3 silencing enhances T-cell activation leading to IL-2 production

Rac1 exerts various actions downstream of the TCR and CD28. It activates actin dynamics and also leads to downstream activation effects leading to transcription factor activation and cytokine gene expression (Macian *et al*, 2001). Therefore, we investigated whether FIP3 silencing affected IL-2 production upon TCR/CD28 engagement. Consistently with our findings on T-cell spreading suggesting Rac1 activation, we observed an enhanced production of IL-2 by FIP3-silenced activated cells (Fig 8A). However, earlier activation events, like Erk1/2 activation, did not appear enhanced but mildly inhibited (Fig 8B), suggesting that FIP3 silencing may have a distinct effect on early and late T-cell activation events, perhaps by increasing the duration of some activation pathways that in turn would lead to enhanced cytokine production.

Altogether, the work we describe here shows that Rac1 is associated with recycling endosomes whose localization and traffic are regulated by Rab11-FIP3. In turn, Rac1 traffic conditions its subcellular localization and local activity, which regulates T-cell spreading and immunological synapse symmetry, as well as T-cell activation leading to cytokine production.

Discussion

Rab11 regulation of vesicle traffic is key for a variety of cellular processes, from nutrient homeostasis to cell division, but its role in immunological synapse formation and T-cell cytoskeleton remodeling has not been explored. Rab11 regulation of endosomal traffic occurs through its association with effector proteins, including the five Rab11-family interacting proteins (Rab11-FIPs) (Horgan & McCaffrey, 2009). Among them, FIP3 displays a Rab11-binding domain common to all five FIPs and several domains that mediate its interaction with molecular motors, like dynein and kinesin, with the Arf6 GTPase, and with vesicular traffic regulators like the ESCRT or the exocyst complex. FIP3 mediates Rab11-controlled traffic of peripheral early endosomes to the pericentrosomal endosomal-recycling compartment (Horgan & McCaffrey, 2009).

Consistent with Rac1 trafficking via Rab11 recycling endosomes, FIP3 overexpression leads to Rac1 accumulation in the pericentrosomal Rab11 compartment. Conversely, FIP3 silencing or overexpression of the FIP3-I^{738}E mutant had the opposite effect, delocalizing Rac1 from centrosomal endosomes to the cytoplasm and the plasma membrane. FIP3 silencing effect on Rac1 subcellular localization was similar to that observed on Rab11 (Fig 1A) and in previous

Figure 6. Rab11-FIP3 regulates T-cell spreading via a Rac1-dependent mechanism.

A–H Jurkat T cells were transfected with control or FIP3.1 siRNA, then transfected again with empty vector or with expression vectors encoding Myc-tagged-Rac1WT, Myc-tagged-Rac1G^{12}V (constitutively active mutant), or Myc-tagged-Rac1T^{17}N (dominant negative mutant). Cells were allowed to spread on poly-lysine-coated coverslips for the indicated time and the spreading area of cells measured. (A–C) Time course plots representing the mean ± SEM of the data shown as in (H). (D–G) Staining for nucleus (blue = DAPI), F-actin (green = phalloidin), and Rac1-Myc (red = anti-Myc) is shown. A single optical section at the level of the contact surface is shown. Scale bar, 10 μm. (H) Population analyses of the spreading area of cells at the level of the contact surface. Dot plots corresponding to measurements at 15 min of spreading. Each dot represents one cell. Horizontal bars represent the mean ± SEM. Mann–Whitney *U*-test. **$P < 0.01$, ****$P < 0.0001$, n.s.: $P \geq 0.05$ non-significant. Data are representative of three experiments.

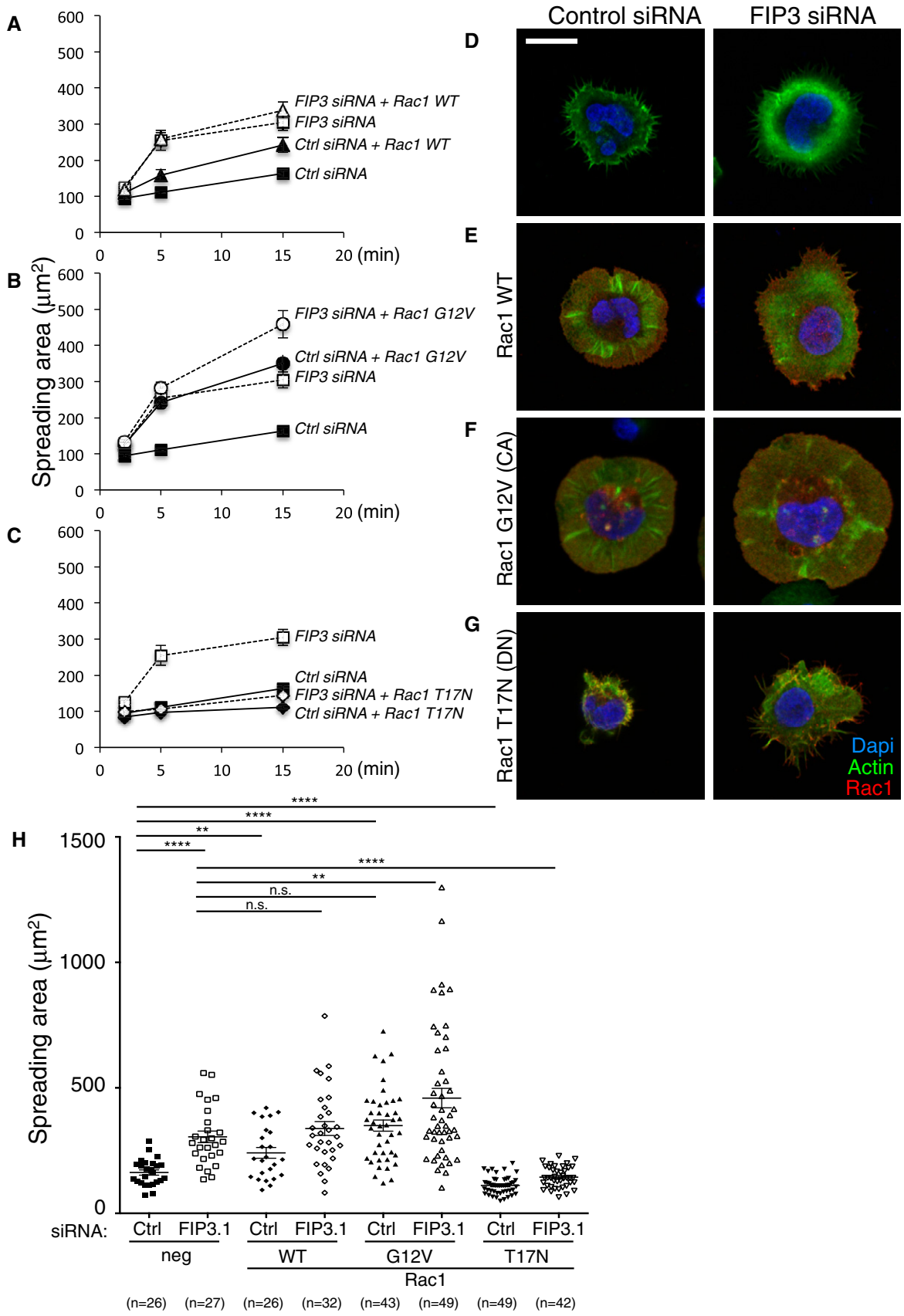

Figure 6.

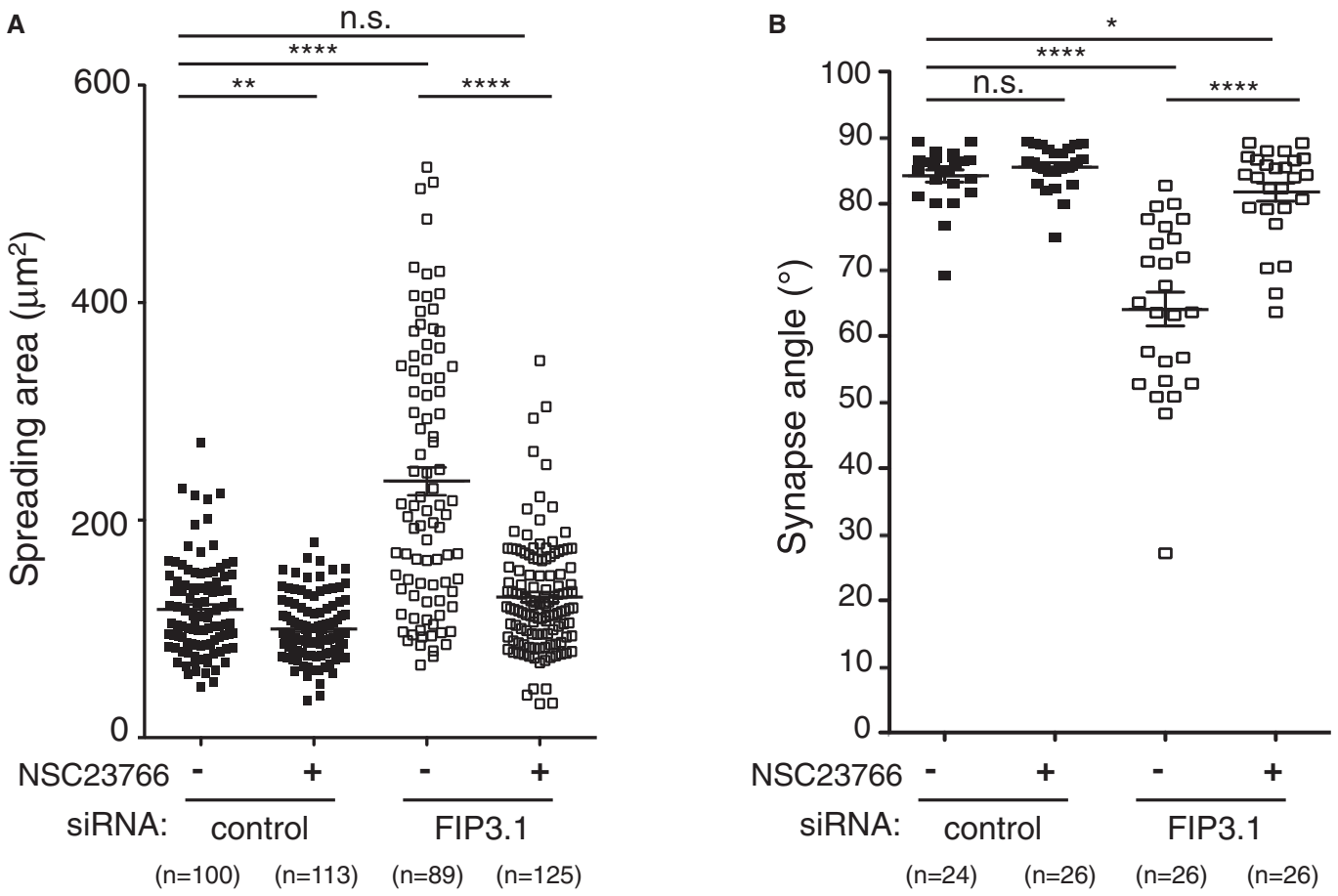

Figure 7. Rac1 inhibitor reverts FIP3-silencing-induced effects on T-cell spreading and synapse symmetry.

A Jurkat T cells transfected with control or FIP3.1 siRNA were treated for 1 h with the Rac1 inhibitor NSC23766 at 100 μM and allowed to spread on poly-lysine-coated coverslips for 15 min. F-actin was detected with FITC-phalloidin, and the spreading area of cells at the contact surface was measured.

B Transfected cells were allowed to form immunological synapses with SEE-pulsed Raji cells for 30 min, and intracellular distribution of Lck was detected by immunofluorescence. Synapse angle was measured as in Fig 4.

Data information: Each dot corresponds to one cell. Horizontal bars represent the mean ± SEM. Mann–Whitney *U*-test. *$P < 0.05$, **$P < 0.01$, ****$P < 0.0001$, n.s.: $P \geq 0.05$ non-significant.

work (Horgan *et al*, 2007), further supporting Rac1 association with Rab11 recycling endosomes.

Interestingly, by immunoprecipitation approaches, we revealed the interaction between Rac1 and FIP3. This interaction was significantly impaired in the FIP3-I^{738}E mutant that does not bind Rab11 (Fig 2C). This is consistent with a tripartite interaction between Rac1, FIP3, and Rab11 that would stabilize Rac1 interaction with FIP3. Rac1 recovery in GFP-FIP3 immunoprecipitates was nevertheless weak, suggesting a low-affinity interaction between these two proteins that may be perturbed by detergent solubilization and dilution. Moreover, these observations, together with those showing that FIP3 silencing strongly diminished Rab11-Rac1 co-localization, suggest that Rac1 and Rab11 may be associated with different endosomal vesicles, linked together via their interaction with FIP3. In this way, Rab11 could regulate Rac1 traffic and subcellular localization (see model in Appendix Fig S3).

FIP3 interacts with microtubule-based molecular motors, like dynein and kinesin (Horgan & McCaffrey, 2009; Horgan *et al*, 2010). These interactions may condition Rab11 vesicle traffic and subcellular localization. The observation that FIP3 silencing disperses Rab11 and Rac1 vesicles all over the cytoplasm would be consistent with an impairment of the interaction of these vesicles with dynein, which, in the presence of FIP3, would drive vesicle movement toward the centrosome. In addition, dynein is involved in microtubule network organization and cell polarization in T lymphocytes forming immunological synapses (Martin-Cofreces *et al*, 2008) and other cells types, like migrating astrocytes (Manneville *et al*, 2010). In our experimental setup, FIP3 silencing did not significantly affect either microtubule network organization, which remained radially organized, or centrosome polarization toward the immunological synapse (Appendix Fig S2). These findings make unlikely that FIP3 silencing affects these dynein functions. Of note, under the same experimental conditions, we observed that the depletion of some polarity regulators, like Dlg1, induced both microtubule network disorganization and impaired centrosome polarization to the immunological synapse (Lasserre *et al*, 2010 and Agüera-Gonzalez, unpublished data).

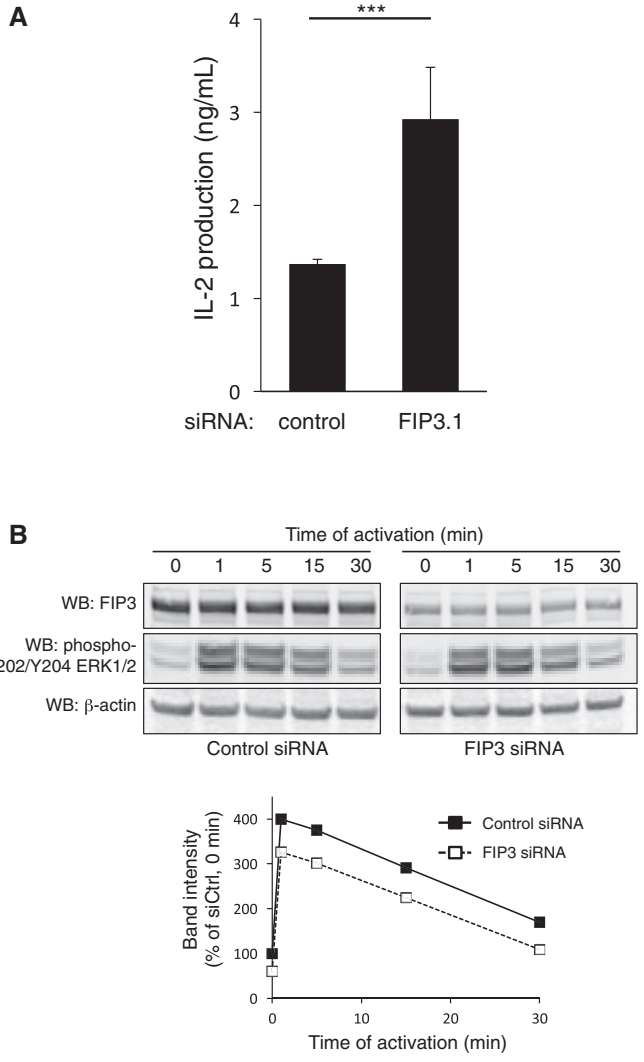

Figure 8. FIP3 silencing enhances IL-2 production.

A Jurkat T cells transfected with control or FIP3.1 siRNA were activated on anti-CD3-coated plastic plates in the presence of soluble anti-CD28 for 16 h. Concentration of IL-2 released in the supernatant was measured by ELISA. Histograms represent the mean ± SD of three experiments. Mann–Whitney *U*-test. ***$P < 0.001$.

B T cells were activated with soluble anti-CD3, and Erk1/2 phosphorylation was analyzed by Western blot. Graph represents the percentage of each band intensity with respect to that of cells transfected with control siRNA and left non-stimulated ($t = 0$). The intensity of each band from Western blot was normalized with respect to the intensity of β-actin for each time point. Representative experiment out of three performed.

Source data are available online for this figure.

Therefore, it appears likely that Rac1 endosomal traffic contributes to balance its concentration and activity in subcellular areas where actin dynamics need to be regulated, like the immunological synapse or lamellipodia. If Rac1 traffic equilibrium is perturbed, actin polymerization may loose its tight control, resulting in the effects described here. Microtubule polarization would direct pericentrosomal recycling endosomes toward the immunological synapse (Das *et al*, 2004), transporting Rac1 to the synapse, and keeping actin dynamics appropriately regulated in that area.

Contrary to FIP3WT and FIP3I^{738}E overexpression that prevented Rac1 clustering at the immunological synapse, FIP3 silencing appeared to have no effect. Nevertheless, Rac1 delivery to FIP3-silenced synapses is likely abnormal, since synapse symmetry was altered. Dustin *et al* proposed that T cells alternate from a polarized asymmetric shape characteristic of migrating cells to a symmetric shape when cells stop and form immunological synapses. Symmetry breaking and relocation is controlled by the equilibrium of signaling molecules downstream of the TCR (Sims *et al*, 2007). T cells may signal at both migratory and stable stages, called kinapses and synapses, respectively (Dustin, 2008). The asymmetric synapses that we observe in FIP3-silenced cells may represent kinapse stages. It is tempting to speculate that controlled endosomal traffic of Rac1 contributes in a yet-unknown way to establish dynamic symmetry changes that help T cells to switch from an asymmetric to a polarized symmetric phenotype.

GTPases are regulated by the balance between guanine nucleotide exchange factors (GEFs), guanine nucleotide-activating proteins (GAPs), and guanine dissociation inhibitors (GDIs) that drive GDP/GTP exchange. GTP-bound active Rac1 regulates effectors that control actin dynamics, like WAVE2. Among the Rac1 GEFs, Vav proteins are key T-cell signaling molecules phosphorylated and activated in response to TCR engagement (Hornstein *et al*, 2004). Other GEFs, like DOCK2, Tiam1 and Trio, also activate Rac1 and may act downstream of the TCR, chemokine receptors, and integrins (Sanui *et al*, 2003; Gronholm *et al*, 2011; van Rijssel & van Buul, 2012). The fact that the Rac inhibitor NSC23766 reverted the effect of FIP3 silencing on T-cell spreading and immunological synapse symmetry would be consistent with an involvement of Tiam1 and/or Trio (Gronholm *et al*, 2011), since NSC23766 competes the interaction of these GEFs with Rac1, but not that of Vav (Gao *et al*, 2004). It is at present unknown whether the subcellular localization of some of these GEFs will be controlled concomitantly with that of Rac1 to drive local actin dynamics. Alternatively, GEF ubiquitous distribution combined with Rac1-redirected localization could drive local actin dynamics. It is worth noting that F-actin distribution in T cells spread on anti-CD3- versus poly-lysine-coated coverslips appeared different, being more peripheral and better defined in anti-CD3-activated cells (Figs 4D and 5A). This might be due to the manner Rac1 encounters its GEFs, either activated by the TCR or distributed in other cellular localizations. In this line, it has been reported that Rab5 overexpression induces Rac1 activation and membrane ruffling in HeLa cells, and concomitant recruitment of Rac1 and its GEF Tiam1 to hypertrophied Rab5-induced early endosomes. It was proposed that Rac1-Tiam1 encountering in early endosomes facilitated local Rac1 activation, actin dynamics, and focal membrane ruffling (Palamidessi *et al*, 2008). These data together with ours suggest that endosomal traffic of Rac1 might facilitate local encountering of Rac1 with its activators and facilitate Rac1 targeting to precise subcellular areas undergoing actin dynamics. Conversely, Rab11 recycling endosomes may keep Rac1 away from the plasma membrane in the pericentrosomal recycling endosomal compartment, buffering Rac1 cortical activation.

We observed that FIP3 silencing enhances IL-2 production, while moderately inhibiting Erk1/2 activation. This effect may be due to a distinct action of RAB11-FIP3 endosomal traffic in early and late T-cell activation events. Lck is associated with the Rab11

compartment (Soares *et al*, 2013a; Bouchet, unpublished data), and FIP3 silencing may have an effect on Lck close effectors differential than that of Rac1. Additionally, Rac1 delocalization and activation of late T-cell signaling events may favor more sustained T-cell activation, resulting in enhanced IL-2 production.

Altogether, the data presented here unveil the fine orchestration between intracellular traffic and actin cytoskeleton regulators through the interplay at recycling endosomes of two of their key regulators, the Rab11 and Rac1 GTPases.

Materials and Methods

Plasmids, siRNA, and antibodies

pEGFP-C1/FIP3 and FIP3-I^{738}E mutant expression vectors were previously described (Horgan *et al*, 2012). pEGFPN1/Rab11 WT and Q^{70}L and S^{25}N mutants were provided by Dr. A. Echard (Institut Pasteur, Paris). pEF-BOS/Rac1-cMyc WT and G^{12}V and T^{17}N mutants were previously described (Komuro *et al*, 1996).

FIP3 was depleted with siRNA duplexes based on human FIP3 sequence described elsewhere: siFIP3.1 (5′-AAGGGATCACAGCCA TCAGAA-3′) (Jing *et al*, 2010) and siFIP3.2 (5′-AAGGCAGTGA GGCGGAGCTGTT-3′) (Wilson *et al*, 2005). Most experiments were performed with siFIP3.1 or lower concentrations of siFIP3.2. The latter is more efficient but also more toxic for the cells.

The following antibodies were used at the concentrations depicted in parenthesis: For Western blots: rabbit anti-FIP3, from Antibodies-online.com (2.4 μg/ml), mouse monoclonal anti-Rac1 (clone 102) from Becton Dickinson (0.1 μg/ml), mouse monoclonal anti-β-tubulin (clone TUB2.1) and anti-β-actin (clone AC-74) from Sigma (1/10,000 dilution), rabbit anti-phospho-Erk (1/2,000 dilution) from Cell Signaling Technology. Secondary antibodies: goat anti-mouse or anti-rabbit Alexa Fluor 680 and goat anti-mouse Alexa Fluor 780 from Molecular Probes (20 ng/ml).

For immunofluorescence: mouse monoclonal IgG2a anti-Rab11 (clone 47) and IgG2b anti-Rac1 (clone 102) from Becton Dickinson (25 and 1 μg/ml, respectively). Mouse monoclonal IgG2b anti-Lck (clone 3A5) from Santa Cruz Biotechnology (2 μg/ml). Mouse monoclonal IgG1 anti-CD3ε (clone UCHT1) from BioLegend Inc (10 μg/ml). Rabbit anti-centrin-3 (1/400 dilution) was a gift from M. Bornens (Institut Curie, France). Mouse IgG2b anti-β-tubulin (clone KMX1) from Millipore (10 μg/ml). FITC-coupled phalloidin from Molecular Probes (1/100 dilution). Secondary antibodies: highly cross-adsorbed Cy3-coupled goat anti-mouse IgG2a and anti-mouse IgG2b from Jackson ImmunoResearch Laboratories (1/100 dilution). FITC-coupled goat anti-mouse IgG1 from SouthernBiotech (0.7 μg/ml). Alexa Fluor 488-coupled goat anti-fluorescein from Molecular Probes (1 μg/ml).

Activation assays: mouse IgG1 anti-CD3ε, clone UCHT1 from BioLegend (500 ng/ml), mouse IgG1 anti-CD28, clone 28.2, from Beckman Coulter (1 μg/ml).

Cell culture and transfection

Human CD4$^+$ T cells were isolated from peripheral blood of healthy donors using the CD4 T Cell Isolation Kit II (Miltenyi Biotec) and cultured in RPMI 1640 medium containing 10% FCS, 1 mM sodium pyruvate, and non-essential amino acids. CD4$^+$ T cells were transfected with 1 nmol of siRNA using a Nucleofector system and the Human T Cell Nucleofector kit (Lonza). Cells were harvested and processed for analysis 72 h after transfection. The human CD4 T-cell line Jurkat clone J77cl20 and the antigen-presenting cells Raji were previously described (Das *et al*, 2004). Jurkat were cultured in RPMI 1640 10% FCS. For siRNA, 2 transfections of 10^7 Jurkat cells were performed at 24-h interval using 2 nmol of either control or FIP3 siRNA with a Neon Transfection system (Life Technologies) (1,400 V, 10 ms, three pulses). Cells were harvested and processed for analysis 72 h after the first transfection. For plasmid transfection, 10 μg of DNA was electroporated in 10^7 Jurkat cells, using the Neon Transfection system, with the same protocol. Cells were harvested and processed for analysis 24 h after DNA transfection.

HEK293T cells were transfected by the calcium phosphate DNA precipitation technique as described (Bouchet *et al*, 2011).

Confocal imaging

For immunological synapse formation, antigen-presenting cells (Raji) were pulsed with 10 μg/ml *Staphylococcus* enterotoxin E superantigen (SEE), then incubated 30 min at 37°C with transfected Jurkat cells in RPMI 1640 medium. Conjugated or isolated cells were plated onto coverslips coated with poly-L-lysine MW: 150–300 kDa, Sigma (0.002% w/v) in water and, after 2 min, fixed in PBS supplemented with 4% paraformaldehyde for 20 min at room temperature. For microtubule detection, T cells activated on anti-CD3-coated coverslips were fixed at RT for 12 min in 4% PFA, rinsed on PBS, and permeabilized for 20 min with 100% methanol at −20°C. After a PBS wash, non-specific binding was prevented by 15-min incubation in PBS with 1% (w/v) bovine serum albumin (PBS-BSA). Coverslips were then incubated for 1 h at room temperature, in PBS-BSA 0.1% (v/v) Triton X-100 and the indicated primary antibody. Coverslips were then rinsed 3 times in PBS-BSA and incubated for 1 h with the corresponding fluorescent-coupled secondary antibody. After three washes in PBS, coverslips were mounted on microscope slides, using 10 μl of ProLong Gold Antifade mounting medium with DAPI (Life Technologies). Confocal microscopy analyses were carried on in a LSM 700 confocal microscope (Zeiss) equipped with a Plan-Apochromat 63× objective. Images acquisition was done with ZEN (Zeiss). Z-stack optical sections were acquired at 0.2-μm-depth increments. Green laser excitation and red laser excitation were intercalated to minimize cross talk between the acquired fluorescence channels.

Co-immunoprecipitation and immunoblot analysis

For immunoprecipitation, 9 million HEK293T cells were lysed in the following lysis buffer: 1% Triton X-100, 50 mM Tris, 140 mM NaCl, 1 mM EGTA, and protease inhibitors (1 mM AEBSF, 10 μg/ml aprotinin, 10 μg/ml leupeptin). Immunoprecipitations of FIP3-GFP constructs were carried out on the cell lysate as described (Bouchet *et al*, 2011), with the use of 30 μl protein-G-agarose beads and 3 μg anti-GFP (7.1/13.1, Roche). Immunoprecipitated proteins were analyzed by Western blot using rabbit monoclonal anti-GFP (clone EPR14104-89, Abcam) or anti-Rac1 (clone 102, Becton Dickinson) antibodies.

Treatment of confocal images

Deconvolution of complete image stacks was performed with Huygens Pro (version 14.10, Scientific Volume Imaging). Colocalization analysis was performed using Fiji software (Schindelin *et al*, 2012) with the *Colocalization Threshold* plugin on the cropped pericentrosomal compartment (Rab11 or FIP3). Threshold was performed using the Costes method autothreshold determination (Costes *et al*, 2004). Pearson's coefficient was calculated for the analysis. Images to quantify Lck or Rac1 accumulation at the immunological synapse were acquired at 1-μm increments in the z-axis to avoid fluorescence overlap. Fluorescence intensity at the synapse was calculated in percentage of the total fluorescence of the cell.

Synapse symmetry

Synapse symmetry was estimated using Lck staining on a mid section by applying the cosine formula on the coordinates of synapse extremities and the coordinates of T cell and APC mass centers (Fig 4B). This allowed to determine the minimal angle formed between the synapse and the two cells.

Analysis of cell spreading

Cells were settled on coverslips coated with poly-L-lysine MW 150–300 kDa (0.002% w/v) in water (Sigma) and incubated at room temperature for the indicated time and fixed in PBS supplemented with 4% paraformaldehyde for 20 min at room temperature. Coverslips were then treated as described above.

Spreading of cells on anti-CD3-coated coverslips (UCHT-1) was performed at 37°C and cells treated in the above-described conditions. Coverslips were precoated with poly-L-lysine, coated with 200 μl of 500 ng/ml mouse IgG1 anti-CD3ε (UCHT1) for 2 h at 37°C, then washed 3× in RPMI. For the measurement of spreading, images were acquired with a 0.5-μm increment in the z-axis. Two contiguous sections starting from the coverslip surface were stacked, surface measure was performed on the phalloidin, or Lck staining using the Fiji *Analyse Particle* feature, on particles larger than 20 μm^2.

Cortical rigidity analysis

Human primary $CD4^+$ T cells (3×10^5 in 100 μl RPMI per condition) were transfected with either control or FIP3 siRNA. Seventy-two hours after transfection, cells were stained for 10 min with 100 nM 5-chloromethylfluorescein diacetate (CMFDA, CellTracker™ Green, Invitrogen), washed twice in RPMI and settled on poly-L-lysine-coated coverslips molecular weight 150–300 kDa (Sigma) (0.002% (w/v) in water), and placed in the wells of a 24-well tissue culture plate. Hundred milliliters of 4% paraformaldehyde was added to the wells, and plates were directly submitted to centrifugation at $3{,}724 \times g$ for 10 min. Coverslips were then washed with PBS and mounted on slides with 10 μl of ProLong Gold Antifade mounting medium. Samples were visualized with a LSM 700 confocal microscope (Carl Zeiss) with a 63× oil-immersion objective, and *z* sections separated by 0.2 μm were acquired. ImageJ was used to build *x-z* images and to determine the maximal sections in "x" (width) and "z" (thickness) axes for each cell (Fig 5F).

Inhibition of Rac1 by NSC23766 inhibitor

Jurkat cells transfected with siRNA control, or siRNA FIP3, were incubated for 1 h at 37°C with or without the Rac inhibitor NSC23766 (Euromedex), diluted in water. Inhibitor was used at 0, 25, 50, and 100 μM. Cells were then assayed for their ability to spread on poly-lysine-coated coverslips for 15 min at 37°C. Cells were fixed and stained with FITC-phalloidin or with anti-Lck, as above. Alternatively, T cells were incubated with SEE superantigen-pulsed Raji cells 30 min at 37°C, set on poly-lysine coverslips, fixed, permeabilized, and stained for Lck, as described above. Immunological synapse confocal microscopy acquisitions and image analyses were carried out as above.

IL-2 production analysis

Ninety-six-well plates were coated or not (control) with 200 μl of 500 ng/ml mouse IgG1 anti-CD3ε (UCHT1) for 2 h at 37°C, then washed 3× in RPMI. Jurkat cells, clone J77cl20 (2.5×10^5 cells in 200 μl) were seeded in wells, in quadruplicate, in the presence or not (control wells) of 1 μg/ml soluble anti-CD28 (clone 28.2). After 16 h of incubation at 37°C, ELISA test was performed on the culture supernatants, following the supplier's instructions (ELISA Human IL-2 DuoSet kit, R&D Systems).

Statistics

Statistical analyses were carried out by the nonparametrical Mann–Whitney *U*-test using Prism software (GraphPad v.6). *P*-values are represented as follows: $****P < 0.0001$; $***P < 0.001$; $**P < 0.01$; $*P < 0.05$; n.s., $P \geq 0.05$, non-significant.

Expanded View for this article is available online.

Acknowledgements

This work was supported by grants from the Agence Nationale de Recherche (ANR, Grant number 11 BSV3 025 01), the Agence National de Recherche sur le SIDA et les Hepatitis Virales (ANRS, Grant number AO 2013-02 CSS1 n°13391/14673), Institut Pasteur, and CNRS. The research leading to these results has received funding from the People Programme (Marie Curie Actions) of the European Union's Seventh Framework Programme FP7/2007-2013/ under the REA grant agreement no. 317057 HOMIN. The Imagopole is part of the France BioImaging infrastructure supported by ANR-10-INSB-04-01, "Investments for the future". Personnel funding was as follows: ANRS and Roux-Institut Pasteur Postdoctoral Fellowships to JB; European Union Marie Curie Actions Initial Training Network HOMIN Predoctoral Fellowship to IdRI, who is a scholar in the Pasteur-Paris University (PPU) International PhD program; Roux-Institut Pasteur and ANR Postdoctoral Fellowships to RL; Fondation ARC pour la Recherche sur le Cancer; and ANR Postdoctoral Fellowships to SAG. We are grateful to Drs. A. Echard and S. Etienne-Manneville (Institut Pasteur, Paris) for expression vectors and reagents, to Dr. F. Niedergang (Institut Cochin, Paris) for critical reading of the manuscript and to Dr. A. Graziani (University Vita e Salute San Raffaele, Milan) for stimulating discussions.

Author contributions

JB designed the project, designed and performed the experiments, analyzed the data, and contributed to writing the manuscript. IdRI performed

experiments, analyzed and discussed data, and critically commented on the manuscript. RL, SAG, and VDB provided expertise, contributed to data analyses and discussions, and critically commented on the manuscript. CC provided technical and organizational support. AD provided expertise and methodology in quantitative image and statistical analyses. MWM provided expression vectors and previous expertise. AA conceived the project, contributed to data analyses and discussions, and wrote the manuscript.

Conflict of interest

The authors declare that they have no conflict of interest.

References

Agüera-Gonzalez S, Bouchet J, Alcover A (2015) *Immunological Synapse*. Chichester: eLS John Wiley & Sons, Ltd

Anton O, Batista A, Millan J, Andres-Delgado L, Puertollano R, Correas I, Alonso MA (2008) An essential role for the MAL protein in targeting Lck to the plasma membrane of human T lymphocytes. *J Exp Med* 205: 3201 – 3213

Bouchet J, Basmaciogullari SE, Chrobak P, Stolp B, Bouchard N, Fackler OT, Chames P, Jolicoeur P, Benichou S, Baty D (2011) Inhibition of the Nef regulatory protein of HIV-1 by a single-domain antibody. *Blood* 117: 3559 – 3568

Bunnell SC, Kapoor V, Trible RP, Zhang W, Samelson LE (2001) Dynamic actin polymerization drives T cell receptor-induced spreading: a role for the signal adaptor LAT. *Immunity* 14: 315 – 329

Burkhardt JK, Carrizosa E, Shaffer MH (2008) The actin cytoskeleton in T cell activation. *Annu Rev Immunol* 26: 233 – 259

Campi G, Varma R, Dustin ML (2005) Actin and agonist MHC-peptide complex-dependent T cell receptor microclusters as scaffolds for signaling. *J Exp Med* 202: 1031 – 1036

Costes SV, Daelemans D, Cho EH, Dobbin Z, Pavlakis G, Lockett S (2004) Automatic and quantitative measurement of protein-protein colocalization in live cells. *Biophys J* 86: 3993 – 4003

Das V, Nal B, Dujeancourt A, Thoulouze MI, Galli T, Roux P, Dautry-Varsat A, Alcover A (2004) Activation-induced polarized recycling targets T cell antigen receptors to the immunological synapse; involvement of SNARE complexes. *Immunity* 20: 577 – 588

Dustin ML (2008) Hunter to gatherer and back: immunological synapses and kinapses as variations on the theme of amoeboid locomotion. *Annu Rev Cell Dev Biol* 24: 577 – 596

Faure S, Salazar-Fontana LI, Semichon M, Tybulewicz VL, Bismuth G, Trautmann A, Germain RN, Delon J (2004) ERM proteins regulate cytoskeleton relaxation promoting T cell-APC conjugation. *Nat Immunol* 5: 272 – 279

Fielding AB, Schonteich E, Matheson J, Wilson G, Yu X, Hickson GR, Srivastava S, Baldwin SA, Prekeris R, Gould GW (2005) Rab11-FIP3 and FIP4 interact with Arf6 and the exocyst to control membrane traffic in cytokinesis. *EMBO J* 24: 3389 – 3399

Finetti F, Paccani SR, Riparbelli MG, Giacomello E, Perinetti G, Pazour GJ, Rosenbaum JL, Baldari CT (2009) Intraflagellar transport is required for polarized recycling of the TCR/CD3 complex to the immune synapse. *Nat Cell Biol* 11: 1332 – 1339

Finetti F, Patrussi L, Galgano D, Cassioli C, Perinetti G, Pazour GJ, Baldari CT (2015) The small GTPase Rab8 interacts with VAMP-3 to regulate the delivery of recycling T-cell receptors to the immune synapse. *J Cell Sci* 128: 2541 – 2552

Gao Y, Dickerson JB, Guo F, Zheng J, Zheng Y (2004) Rational design and characterization of a Rac GTPase-specific small molecule inhibitor. *Proc Natl Acad Sci USA* 101: 7618 – 7623

Gronholm M, Jahan F, Marchesan S, Karvonen U, Aatonen M, Narumanchi S, Gahmberg CG (2011) TCR-induced activation of LFA-1 involves signaling through Tiam1. *J Immunol* 187: 3613 – 3619

Hashimoto-Tane A, Yokosuka T, Sakata-Sogawa K, Sakuma M, Ishihara C, Tokunaga M, Saito T (2011) Dynein-driven transport of T cell receptor microclusters regulates immune synapse formation and T cell activation. *Immunity* 34: 919 – 931

Horgan CP, Oleksy A, Zhdanov AV, Lall PY, White IJ, Khan AR, Futter CE, McCaffrey JG, McCaffrey MW (2007) Rab11-FIP3 is critical for the structural integrity of the endosomal recycling compartment. *Traffic* 8: 414 – 430

Horgan CP, McCaffrey MW (2009) The dynamic Rab11-FIPs. *Biochem Soc Trans* 37: 1032 – 1036

Horgan CP, Hanscom SR, Jolly RS, Futter CE, McCaffrey MW (2010) Rab11-FIP3 links the Rab11 GTPase and cytoplasmic dynein to mediate transport to the endosomal-recycling compartment. *J Cell Sci* 123: 181 – 191

Horgan CP, Hanscom SR, Kelly EE, McCaffrey MW (2012) Tumor susceptibility gene 101 (TSG101) is a novel binding-partner for the class II Rab11-FIPs. *PLoS ONE* 7: e32030

Hornstein I, Alcover A, Katzav S (2004) Vav proteins, masters of the world of cytoskeleton organization. *Cell Signal* 16: 1 – 11

Jing J, Junutula JR, Wu C, Burden J, Matern H, Peden AA, Prekeris R (2010) FIP1/RCP binding to Golgin-97 regulates retrograde transport from recycling endosomes to the trans-Golgi network. *Mol Biol Cell* 21: 3041 – 3053

Komuro R, Sasaki T, Takaishi K, Orita S, Takai Y (1996) Involvement of Rho and Rac small G proteins and Rho GDI in Ca^{2+}-dependent exocytosis from PC12 cells. *Genes Cells* 1: 943 – 951

Kupfer A, Mosmann TR, Kupfer H (1991) Polarized expression of cytokines in cell conjugates of helper T cells and splenic B cells. *Proc Natl Acad Sci USA* 88: 775 – 779

Larghi P, Williamson DJ, Carpier JM, Dogniaux S, Chemin K, Bohineust A, Danglot L, Gaus K, Galli T, Hivroz C (2013) VAMP7 controls T cell activation by regulating the recruitment and phosphorylation of vesicular Lat at TCR-activation sites. *Nat Immunol* 14: 723 – 731

Lasserre R, Charrin S, Cuche C, Danckaert A, Thoulouze MI, de Chaumont F, Duong T, Perrault N, Varin-Blank N, Olivo-Marin JC, Etienne-Manneville S, Arpin M, Di Bartolo V, Alcover A (2010) Ezrin tunes T-cell activation by controlling Dlg1 and microtubule positioning at the immunological synapse. *EMBO J* 29: 2301 – 2314

Le Floc'h A, Tanaka Y, Bantilan NS, Voisinne G, Altan-Bonnet G, Fukui Y, Huse M (2013) Annular PIP3 accumulation controls actin architecture and modulates cytotoxicity at the immunological synapse. *J Exp Med* 210: 2721 – 2737

Macian F, Lopez-Rodriguez C, Rao A (2001) Partners in transcription: NFAT and AP-1. *Oncogene* 20: 2476 – 2489

Manneville JB, Jehanno M, Etienne-Manneville S (2010) Dlg1 binds GKAP to control dynein association with microtubules, centrosome positioning, and cell polarity. *J Cell Biol* 191: 585 – 598

Martin-Cofreces NB, Robles-Valero J, Cabrero JR, Mittelbrunn M, Gordon-Alonso M, Sung CH, Alarcon B, Vazquez J, Sanchez-Madrid F (2008) MTOC translocation modulates IS formation and controls sustained T cell signaling. *J Cell Biol* 182: 951 – 962

Martin-Cofreces NB, Baixauli F, Lopez MJ, Gil D, Monjas A, Alarcon B, Sanchez-Madrid F (2012) End-binding protein 1 controls signal propagation from the T cell receptor. *EMBO J* 31: 4140 – 4152

Nguyen K, Sylvain NR, Bunnell SC (2008) T cell costimulation via the integrin VLA-4 inhibits the actin-dependent centralization of signaling microclusters containing the adaptor SLP-76. *Immunity* 28: 810 – 821

Palamidessi A, Frittoli E, Garre M, Faretta M, Mione M, Testa I, Diaspro A, Lanzetti L, Scita G, Di Fiore PP (2008) Endocytic trafficking of Rac is required for the spatial restriction of signaling in cell migration. *Cell* 134: 135 – 147

Patino-Lopez G, Dong X, Ben-Aissa K, Bernot KM, Itoh T, Fukuda M, Kruhlak MJ, Samelson LE, Shaw S (2008) Rab35 and its GAP EPI64C in T cells regulate receptor recycling and immunological synapse formation. *J Biol Chem* 283: 18323 – 18330

van Rijssel J, van Buul JD (2012) The many faces of the guanine-nucleotide exchange factor trio. *Cell Adh Migr* 6: 482 – 487

Roumier A, Olivo-Marin JC, Arpin M, Michel F, Martin M, Mangeat P, Acuto O, Dautry-Varsat A, Alcover A (2001) The membrane-microfilament linker ezrin is involved in the formation of the immunological synapse and in T cell activation. *Immunity* 15: 715 – 728

Sanui T, Inayoshi A, Noda M, Iwata E, Oike M, Sasazuki T, Fukui Y (2003) DOCK2 is essential for antigen-induced translocation of TCR and lipid rafts, but not PKC-theta and LFA-1, in T cells. *Immunity* 19: 119 – 129

Schindelin J, Arganda-Carreras I, Frise E, Kaynig V, Longair M, Pietzsch T, Preibisch S, Rueden C, Saalfeld S, Schmid B, Tinevez JY, White DJ, Hartenstein V, Eliceiri K, Tomancak P, Cardona A (2012) Fiji: an open-source platform for biological-image analysis. *Nat Methods* 9: 676 – 682

Sims TN, Soos TJ, Xenias HS, Dubin-Thaler B, Hofman JM, Waite JC, Cameron TO, Thomas VK, Varma R, Wiggins CH, Sheetz MP, Littman DR, Dustin ML (2007) Opposing effects of PKCtheta and WASp on symmetry breaking and relocation of the immunological synapse. *Cell* 129: 773 – 785

Soares H, Henriques R, Sachse M, Ventimiglia L, Alonso MA, Zimmer C, Thoulouze MI, Alcover A (2013a) Regulated vesicle fusion generates signaling nanoterritories that control T cell activation at the immunological synapse. *J Exp Med* 210: 2415 – 2433

Soares H, Lasserre R, Alcover A (2013b) Orchestrating cytoskeleton and intracellular vesicle traffic to build functional immunological synapses. *Immunol Rev* 256: 118 – 132

Steffen A, Koestler SA, Rottner K (2014) Requirements for and consequences of Rac-dependent protrusion. *Eur J Cell Biol* 93: 184 – 193

Valitutti S, Dessing M, Aktories K, Gallati H, Lanzavecchia A (1995) Sustained signaling leading to T cell activation results from prolonged T cell receptor occupancy. Role of T cell actin cytoskeleton. *J Exp Med* 181: 577 – 584

Welz T, Wellbourne-Wood J, Kerkhoff E (2014) Orchestration of cell surface proteins by Rab11. *Trends Cell Biol* 24: 407 – 415

Wilson GM, Fielding AB, Simon GC, Yu X, Andrews PD, Hames RS, Frey AM, Peden AA, Gould GW, Prekeris R (2005) The FIP3-Rab11 protein complex regulates recycling endosome targeting to the cleavage furrow during late cytokinesis. *Mol Biol Cell* 16: 849 – 860

